Yong Hwan Han,[1] Márcio Buffolo,[1] Karla Maria Pires,[1] Shaobo Pei,[1] Philipp E. Scherer,[2,3] and Sihem Boudina[1]

Adipocyte-Specific Deletion of Manganese Superoxide Dismutase Protects From Diet-Induced Obesity Through Increased Mitochondrial Uncoupling and Biogenesis

Diabetes 2016;65:2639–2651 | DOI: 10.2337/db16-0283

Obesity and insulin resistance are associated with oxidative stress (OS). The causal role of adipose OS in the pathogenesis of these conditions is unknown. To address this issue, we generated mice with an adipocyte-selective deletion of manganese superoxide dismutase (MnSOD). When fed a high-fat diet (HFD), the AdSod2 knockout (KO) mice exhibited less adiposity, reduced adipocyte hypertrophy, and decreased circulating leptin. The resistance to diet-induced adiposity was the result of an increased metabolic rate and energy expenditure. Furthermore, palmitate oxidation was elevated in the white adipose tissue (WAT) and brown adipose tissue of AdSod2 KO mice fed an HFD, and the expression of key fatty acid oxidation genes was increased. To gain mechanistic insight into the increased fat oxidation in HFD-fed AdSod2 KO mice, we quantified the mitochondrial function and mitochondrial content in WAT and found that MnSOD deletion increased mitochondrial oxygen consumption and induced mitochondrial biogenesis. This effect was preserved in cultured adipocytes from AdSod2 KO mice in vitro. As expected from the enhanced fat oxidation, circulating levels of free fatty acids were reduced in the HFD-fed AdSod2 KO mice. Finally, HFD-fed AdSod2 KO mice were protected from hepatic steatosis, adipose tissue inflammation, and glucose and insulin intolerance. Taken together, these results demonstrate that MnSOD deletion in adipocytes triggered an adaptive stress response that activated mitochondrial biogenesis and enhanced mitochondrial fatty acid oxidation, thereby preventing diet-induced obesity and insulin resistance.

Oxidative stress (OS) occurs when reactive oxygen species (ROS) production exceeds the detoxification rate in the cell, which promotes damage to various biomolecules, such as nucleic acids, lipids, and proteins. Obesity is one of multiple conditions associated with OS (1). In addition to increased systemic biomarkers of OS, obese humans and animals exhibit increased adipose tissue OS, as evidenced by higher hydrogen peroxide (H_2O_2) production, reduced antioxidant defense mechanisms, enhanced NADPH oxidase activity, and elevated oxidative damage to proteins (2–4). Although the link between OS and obesity has been established, whether mitochondrial ROS plays a causal role in fat accumulation in vivo is unknown.

Studies have attempted to address this important question and have yielded conflicting results because of the complexity of using animal models with whole-body deletion or overexpression of mitochondrial ROS-generating or scavenging enzymes. For example, knockout (KO) of the mitochondrial-specific peroxidase peroxiredoxin 3 (Prx3) enhances H_2O_2 production and promoted fat accumulation in mice (5). Similarly, mice lacking the redox-sensitive protein $p66^{Shc}$, which produces H_2O_2 through the oxidation of cytochrome c in the mitochondria (6), exhibits reduced fat accumulation and increased energy expenditure

[1]Department of Nutrition and Integrative Physiology; Division of Endocrinology, Metabolism and Diabetes; and Program in Molecular Medicine, University of Utah School of Medicine, Salt Lake City, UT
[2]Touchstone Diabetes Center, Department of Internal Medicine, University of Texas Southwestern Medical Center, Dallas, TX
[3]Department of Cell Biology, University of Texas Southwestern Medical Center, Dallas, TX

Corresponding author: Sihem Boudina, sihem.boudina@hmbg.utah.edu.

Received 2 March 2016 and accepted 25 May 2016.

This article contains Supplementary Data online at http://diabetes.diabetesjournals.org/lookup/suppl/doi:10.2337/db16-0283/-/DC1.

(EE) (7). By contrast, mice with whole-body overexpression of manganese superoxide dismutase (MnSOD) or mitochondria-targeted human catalase develop the same degree of obesity and insulin resistance when maintained on a high-fat diet (HFD) (8,9). Furthermore, emerging evidence has revealed that mitochondrial ROS in the form of H_2O_2 is a prerequisite for the adipogenesis of mesenchymal stem cells in vitro (10), thus making the distinction between the effects of ROS on adipogenesis versus their role in adipocyte function almost impossible. Finally, the results from these studies could have been confounded by the contribution of other tissues (i.e., skeletal muscle) to whole-body energy homeostasis or by the modulation of inflammatory pathways in adipose tissue due to changes in the redox status of macrophages.

To circumvent these limitations and to directly assess the role of mitochondrial superoxide generation in adipocyte functions, whole-body energy homeostasis, and insulin sensitivity, we generated mice with an adipocyte-targeted deletion of *Sod2* (MnSOD), which is the primary superoxide-scavenging enzyme that catalyzes the dismutation of the superoxide radical (O_2^-) to H_2O_2 and molecular oxygen in the mitochondrial matrix. We reveal that MnSOD deletion in adipocytes is protective against HFD-induced weight gain and insulin resistance through the stimulation of mitochondrial function and biogenesis, thereby allowing the clearance of fatty acids (FAs).

RESEARCH DESIGN AND METHODS

Generation of AdSod2 KO Mice

Mice carrying the adiponectin promoter-*Cre* transgene were bred with mice carrying a floxed *Sod2* allele that contained LoxP sites surrounding exon 3 of the *Sod2* gene (obtained through the Animal Models of Diabetes Complications Consortium). The resultant adiponectin-*Cre*; $Sod2^{f/f}$ mice (hereafter referred to as AdSod2 KO mice) on a C57BL/6J background were housed in a mouse facility on a 12-h light-dark cycle in a 22°C temperature-controlled room. The animals were maintained on a normal chow diet (NCD) containing 10% calories from fat, 20% calories from protein, and 69% calories from carbohydrates (N 8806; Harlan Laboratories) or subjected to a high-fat, high-sucrose diet containing 45% calories from fat, 19% calories from protein, and 36% calories from carbohydrates (N 06415; Harlan Laboratories) starting at 8 weeks of age. Animal care and study protocols were approved by the Institutional Animal Care and Use Committee of the University of Utah and were in accordance with National Institutes of Health guidelines.

Superoxide Measurements

Mitochondrial superoxide production was measured in isolated adipocytes by electron paramagnetic resonance spectroscopy using the superoxide spin-trapping reagent CMH (1-hydroxy-3-methoxycarbonyl-2,2,5,5-tetramethylpyrrolidine) as previously described (11). In addition, we used CMH to measure superoxide levels in differentiated adipose progenitors (APs) using flow cytometry.

Histology and Morphometric Measurements

White adipose tissue (WAT) represented by the inguinal (iWAT) and epididymal (eWAT) depots and interscapular brown adipose tissue (BAT) were obtained from AdSod2 KO mice or wild-type (WT) control mice fed either the NCD or the HFD for 21 weeks. The samples were fixed in 4% paraformaldehyde for 48 h, embedded in paraffin, cut into 5-μm sections, and stained with hematoxylin and eosin. The adipocyte diameter was determined as previously described (12). The total number of adipocytes was measured using cellSens software (Olympus, Waltham, MA). The adipocyte number per area in millimeters squared was averaged from at least 500 adipocytes counted among 10 images per animal. Liver samples were snap frozen in liquid nitrogen, embedded in optimal cutting temperature medium, sectioned with a 10-μm thickness, mounted on slides, and allowed to dry for 1–2 h. The sections were stained with Oil Red O as previously described (13).

Immunofluorescence Staining

Paraffin-embedded eWAT sections were stained with an anti-F4/80 antibody to detect macrophages in the adipose tissue. Uncoupling protein (UCP)-1 immunoreactivity was assessed in paraffin-embedded BAT sections (Supplementary Data). The images were acquired with an XM10 Olympus fluorescence camera. F4/80/DAPI and immunofluorescence staining was quantified based on color intensity using cellSens software. UCP-1/DAPI immunofluorescence staining was quantified based on color intensity using cellSens software in representative nonconsecutive fields per slide from two slides per animal in a blinded fashion.

Indirect Calorimetry and Locomotor Activity

Mice were housed in a four-chamber Oxymax Comprehensive Lab Animal Monitoring System (CLAMS) (Columbus Instruments, Columbus, OH) as previously described (14). The O_2 and CO_2 content of the exhaust air from each chamber were compared with the ambient air O_2 and CO_2 content. Food consumption was monitored by using an electronic scale, water by an electronic sipper tube, and movement by XY/Z laser beam interruption. The respiratory exchange ratio (RER) was calculated as VCO_2/VO_2, and EE was calculated as heat/body weight.

Glucose Tolerance Test, Insulin Tolerance Test, Serum Metabolites, and Hormone Levels

Glucose tolerance tests (GTTs) were performed after a 6-h fast, and insulin tolerance tests were performed on random-fed animals by injecting insulin (0.75 units/kg body weight) as previously described (14). Insulin concentrations were determined using a sensitive rat insulin radioimmunoassay kit (Linco Research, St. Charles, MO). Free fatty acid (FFA) concentrations were determined using the Half Micro Test kit (Roche Diagnostics, Mannheim, Germany), and triglyceride concentrations were determined using a Serum Triglyceride Determination Kit (Sigma-Aldrich, St. Louis, MO). Serum leptin and adiponectin levels were determined using ELISA kits

from EMD Millipore (Billerica, MA) and R&D Systems (Minneapolis, MN), respectively.

FA Oxidation

Palmitate oxidation was measured as previously described (15). Briefly, freshly isolated fat and hindlimb muscle were incubated in medium containing 2% BSA, 0.3 mmol/L palmitic acid, and 20 μCi [9,10-^{3}H]palmitic acid. After 2 h, palmitic acid oxidation was assessed by measuring ^3H_2O production in the incubation medium. The media was extracted by the addition of 2.5 mL of methanol/chloroform (1:2 volume for volume) and 1 mL of 2 mol/L KCl/HCl (1:1 volume for volume) followed by centrifugation at 3,000*g* for 15 min. ^3H_2O release in the aqueous phase was measured by liquid scintillation counting. Background ^3H_2O release was measured in an aliquot of medium with [9,10-^{3}H]palmitic acid that was incubated without tissue.

Mitochondrial Oxygen Consumption

The adipose tissue oxygen consumption rate (OCR) was assessed by using freshly isolated mouse BAT, iWAT, and eWAT. These tissues were rinsed with nonbuffered Krebs-Henseleit buffer media containing 111 mmol/L NaCl, 4.7 mmol/L KCl, 2 mmol/L $MgSO_4$, 1.2 mmol/L Na_2HPO_4, 0.5 mmol/L of carnitine, and 2.5 mmol/L glucose. They were then cut into pieces (~10 mg) and washed extensively. Each piece was placed into a single well of an XF24 Islet Capture Microplate (Seahorse Bioscience, North Billerica, MA) and covered with a customized screen that allowed free perfusion while minimizing tissue movement. Krebs-Henseleit buffer was added to each well, and OCR was measured. Oligomycin (10 μmol/L) was added to inhibit ATP synthesis, and carbonyl cyanide-*p*-trifluoromethoxyphenylhydrazone (FCCP) (20 μmol/L) was supplied to artificially uncouple the mitochondria. Each OCR value was an average of three independent pieces per mouse per experiment.

Mitochondrial DNA Quantification

Mitochondrial DNA (mtDNA) was quantified as previously described (16). Briefly, total genomic DNA was isolated from the BAT or iWAT of WT and AdSod2 KO mice fed NCD or HFD by using a Gentra Puregene Tissue Kit (QIAGEN, Valencia, CA). Tubulin was PCR amplified from the genomic DNA by using the primers 5′-CCAGCCTCCCACTGTGG-3′ and 5′-CATGCCTTCTCCCACGTAC-3′. NADH dehydrogenase subunit 1 was PCR amplified from the mtDNA by using the primers 5′-ACCATTTGCAGACGCCATAA-3′ and 5′-TGAAATTGTTTGGGCTACGG-3′.

Mitochondrial Volume Density

Samples were collected from freshly excised iWAT, fixed in 2.5% glutaraldehyde and 1% paraformaldehyde, post-fixed in 2% osmium, embedded in resin, and sectioned (80- to 100-nm thick). The morphometric analysis was performed using blind counting to determine the mitochondrial density and was expressed as the number per area. Three sections were counted per animal.

Quantitative RT-PCR

Total RNA was isolated with TRIzol (Life Technologies, Grand Island, NY) according to the manufacturer's instructions. For the quantitative PCR, the final reaction volume was 10 μL and included specific primers (Supplementary Table 1), 10 ng of cDNA, and SYBR Green Master Mix (Life Technologies). The real-time PCR assays were run on an ABI Prism 7900HT Real-Time PCR System (Applied Biosystems). Normalization was performed using ribosomal protein L13 (*Rpl13*) RNA. Quantification was performed by using the comparative ΔCt method.

Western Blotting

Cells were homogenized in cell lysis buffer (30 mmol/L HEPES [pH 7.4], 1% NP-40, 1 mmol/L EDTA, 1 mmol/L dithiothreitol, 10% glycerol, and protease inhibitor cocktail [Sigma, St. Louis, MO]). The protein concentration was measured using a Micro BCA Protein Assay Reagent (Pierce, Rockford, IL). The protein extracts were resolved by SDS-PAGE and electrotransferred onto an Immobilon polyvinylidene fluoride membrane (Millipore, Bedford, MA). The membranes were probed with the following primary antibodies: MnSOD; Tom20 (Santa Cruz Biotechnology); succinate dehydrogenase subunit A (SDHA), phospho–dynamin-related protein (DRP1) (Ser637), DRP1, mitofusin 1 (MFN-1), TXNIP, GLUT1, GAPDH, and tubulin (Cell Signaling Technology, Danvers, MA); 4-hydroxynonenal (4-HNE) (Abcam, Cambridge, MA); and glutathione peroxidase 4 (GPX4) (R&D Systems). Alexa Fluor anti-rabbit 680 (Invitrogen, Carlsbad, CA) and anti-mouse 800 (VWR International, West Chester, PA) were used as the secondary antibodies. Fluorescence was quantified by using the Odyssey imager (LI-COR Biosciences, Lincoln, NE).

Statistical Analysis

All data are expressed as mean ± SEM. The results were assessed by unpaired Student *t* or one-way ANOVA test using Prism 5 software (GraphPad Software, La Jolla, CA). $P < 0.05$ was considered significant.

RESULTS

MnSOD Deletion in Adipocytes Enhances Superoxide Generation

AdSod2 KO mice were born at a normal Mendelian ratio and viable. As shown in Fig. 1*A* and *B*, the MnSOD protein (normalized to mitochondrial SDHA) was absent in adipocytes isolated from the iWAT and eWAT of AdSod2 KO mice. Because brown adipocytes contain more mitochondria and due to BAT atrophy in KO mice, we measured MnSOD protein expression in whole BAT homogenates. MnSOD protein expression was significantly reduced in KO mice (Fig. 1*C*). By contrast, MnSOD expression was preserved in other mitochondria-rich tissues, such as the heart (Supplementary Fig. 1*E* and *F*). As expected from the absent MnSOD, superoxide generation was enhanced in the iWAT adipocytes of AdSod2 KO mice fed the NCD compared with that in WT mice fed the same diet (Fig. 1*D*). Of note, superoxide generation in iWAT adipocytes

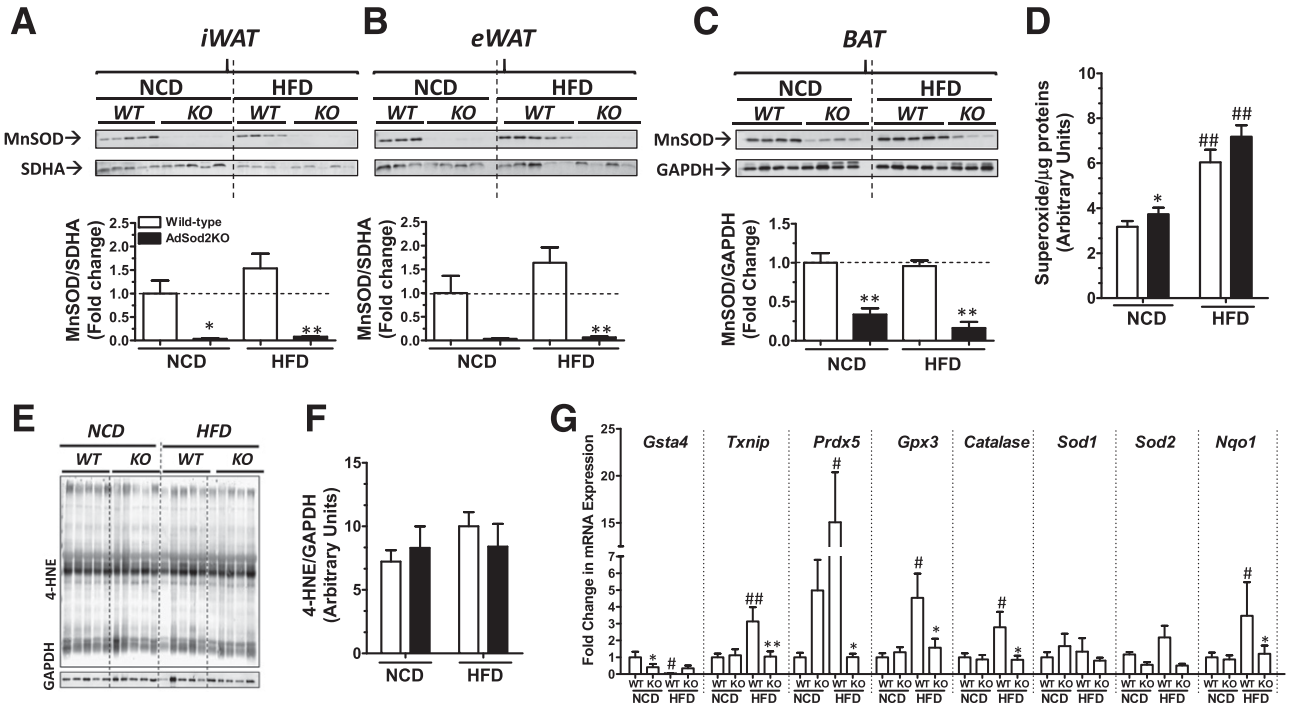

Figure 1—MnSOD deletion in adipocytes increased superoxide generation but did not enhance lipid peroxidation. Representative Western blots and the corresponding densitometry of MnSOD protein expression normalized by SDHA expression in isolated adipocytes from iWAT (*A*) and eWAT (*B*). MnSOD protein expression normalized GAPDH protein expression in whole interscapular BAT homogenates (*C*). *D*: Superoxide levels in isolated adipocytes from iWAT of WT or AdSod2 KO mice fed an NCD or HFD for 21 weeks. *E*: Representative Western blot of 4-HNE and GAPDH protein expression in iWAT. *F*: Densitometry of 4-HNE normalized by GAPDH. *G*: Relative mRNA expression of major antioxidant enzymes in iWAT. n = 3–6 mice per group. Data are mean ± SEM. *$P < 0.05$, **$P < 0.005$ vs. WT under the same feeding condition; #$P < 0.05$, ##$P < 0.005$ vs. NCD within the same genotype.

was similarly induced by HFD feeding in both the WT and the KO mice (Fig. 1*D*). Superoxide levels were increased in eWAT adipocytes of AdSod2 KO mice independent of the diet, but the difference did not reach statistical significance (Supplementary Fig. 2*A*).

Next, we investigated whether the increase in superoxide levels promoted protein carbonylation by measuring 4-HNE Michael protein adducts, but we found no significant differences in either iWAT, eWAT, or BAT between groups (Fig. 1*E* and *F* and Supplementary Fig. 2*B–E*). To test whether the absence of MnSOD triggered a compensatory induction of the antioxidant response, we examined the mRNA levels of key antioxidant enzymes. Clear differences in HFD-mediated modulation of antioxidant enzyme expression were observed between the iWAT and eWAT. The expression of most antioxidant enzymes was induced by HFD feeding in the iWAT and reduced in the eWAT, with the exception of glutathione *S*-transferase α4 (*Gsta4*), which was similarly reduced by HFD feeding in both depots (Fig. 1*G* and Supplementary Fig. 2*F*). Despite the increase in superoxide generation, we did not observe a compensatory increase in the mRNA levels of antioxidant enzymes in the iWAT or eWAT of the AdSod2 KO mice, except a modest increase in *Sod1* mRNA in the eWAT was found (Supplementary Fig. 2*F*). Although *Gsta4* mRNA levels were elevated in the iWAT and eWAT of the HFD-fed AdSod2 KO mice compared with that in the diet-matched WT mice, the difference was not significant. Finally, the expression of enzymes involved in the detoxification of H_2O_2, such as catalase or GPX4, were either unchanged (data not shown) or reduced in the KO mice (Supplementary Fig. 1*G–M*).

Absent Adipocyte MnSOD Attenuates Diet-Induced Adiposity

To investigate the impact of mitochondrial superoxide generation on whole-body physiology and metabolism, AdSod2 KO mice were studied both on an NCD and after exposure to an HFD starting at 8 weeks of age for 21 weeks. The HFD induced a 50% increase in weight gain in the WT mice compared with only a 26% increase in the AdSod2 KO mice (Fig. 2*B*). Thus, the body weights at kill were significantly reduced in the HFD-fed AdSod2 KO mice compared with the WT mice fed the HFD (Fig. 2*A*). Similarly, the iWAT and eWAT weights normalized to the body weights were smaller in the KO mice than in the WT mice fed the HFD (Fig. 2*C* and *D*). We observed significant atrophy of the BAT in the KO versus the WT mice, independent of the diet (Fig. 2*E* and Supplementary Fig. 3*A*). However, the BAT morphology of the KO mice was denser and contained fewer lipid droplets, especially under HFD conditions (Supplementary Fig. 3*B*). The WAT

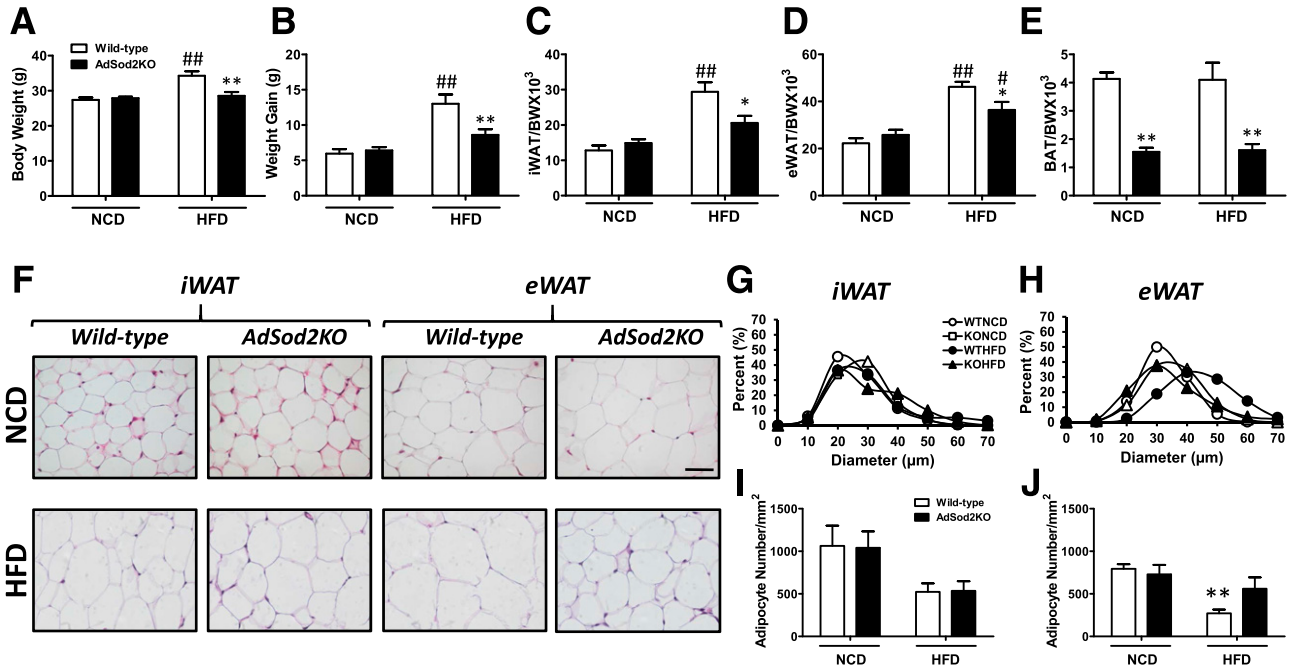

Figure 2—MnSOD deficiency in adipocytes reduced diet-induced weight gain and adiposity. Body weights (*A*), weight gain (*B*), iWAT weight/body weight (BW) × 10^3 (*C*), eWAT weight/BW × 10^3 (*D*), BAT weight/BW × 10^3 (*E*) in WT or AdSod2 KO mice maintained on NCD or HFD for 21 weeks. *F*: Representative images of iWAT and eWAT sections stained with hematoxylin and eosin. *G* and *H*: Distribution of adipocyte diameter in iWAT and eWAT, respectively. *I* and *J*: Adipocyte number per area in iWAT and eWAT, respectively. n = 12–18 mice per group for *A*–*E*. Ten images per animal were used to quantify adipocyte diameter and number for five to six mice per group. Scale bar = 40 μm. Data are mean ± SEM. **P* < 0.05, ***P* < 0.005 vs. WT under the same feeding condition; #*P* < 0.05, ##*P* < 0.005 vs. NCD within the same genotype.

morphometric analysis revealed a reduction in adipocyte diameters, with no change in adipocyte numbers in the eWAT of the AdSod2 KO mice compared with that of the WT mice on the HFD (Fig. 2*F*–*J*). Consistent with the reduced adipocyte hypertrophy, the circulating leptin concentration was increased in the HFD-fed WT mice but significantly decreased (>70%) in the HFD-fed KO mice (Table 1). These data suggest that MnSOD deletion in adipocytes attenuates diet-induced adiposity and reduces adipocyte hypertrophy.

Metabolic Rate and EE Increase in AdSod2 KO Mice on an HFD

To better understand why the AdSod2 KO mice remained lean when fed an HFD, we assessed the whole-body EE at 23°C after 12 weeks of the HFD using CLAMS. Of note, the KO mice were leaner even after 12 weeks of HFD feeding, as evidenced by reduced body weights and fat masses, compared with the WT mice on the HFD (Supplementary Fig. 7*A*–*C*). Compared with WT mice on the HFD, the AdSod2 KO mice on the HFD exhibited increased metabolic rates, as evidenced by the increase in VO_2 and VCO_2 both at night (Fig. 3*A* and *B*) and during the day (Supplementary Fig. 4*A* and *B*). Because of the proportional increases observed in VO_2 and VCO_2 in the HFD-fed AdSod2 KO mice at night, the RER was the same as that in the HFD-fed WT mice. This value was reduced compared with the value observed for the NCD-fed animals, suggesting preferential FA utilization (Fig. 3*C* and Supplementary Fig. 4*C*). Finally, the EE was reduced in the HFD-fed WT mice but increased in the AdSod2 KO mice on the same diet (Fig. 3*D* and Supplementary Fig. 4*D*). Thus, the protection of the AdSod2 KO mice from diet-induced adiposity could be due to an increased metabolic rate and EE and is not caused by an increase in food intake or activity.

HFD-Fed AdSod2 KO Mice Maintain an Increased Metabolic Rate When Housed at Thermoneutrality

Due to BAT atrophy and reduced adiposity in the AdSod2 KO mice, we examined whether the increase in the metabolic rate observed in the KO mice (especially under HFD feeding) was a result of a compensatory increase in adaptive thermogenesis. Thus, we measured the basal body temperature at 22°C and found no difference between groups (Supplementary Fig. 3*C*). Next, we subjected the WT and AdSod2 KO mice fed either the NCD or the HFD to an acute cold challenge and found that the KO mice were cold intolerant independent of the diet (Supplementary Fig. 3*D*), which is likely due to reduced insulation and/or BAT atrophy. To directly test the possibility that the KO mice increased their EE as a result of increased adaptive thermogenesis to maintain their body temperature, we subjected the mice to the NCD or HFD for 8 weeks and

Table 1—Serum metabolites, hormones, and lipids in WT and AdSod2 KO mice fed NCD or HFD

	NCD		HFD	
	WT	AdSod2 KO	WT	AdSod2 KO
Glucose (mg/dL)	109.9 ± 8.1	99.3 ± 10.8	146 ± 6.3##	129.8 ± 5.9#
T_0 insulin (ng/mL)	0.34 ± 0.06	0.3 ± 0.06	0.54 ± 0.06	0.21 ± 0.03**
T_{30} insulin (ng/mL)	0.48 ± 0.09	0.47 ± 0.1	0.47 ± 0.08	0.35 ± 0.05
Leptin (ng/mL)	5 ± 0.5	5.4 ± 0.8	14.6 ± 4.3	4.1 ± 0.9*
Adiponectin (ng/mL)	7,443.1 ± 505.1	7,242.1 ± 504.8	6,890 ± 413.8	7,183 ± 579.6
FFA (mmol/L)	0.46 ± 0.03	0.63 ± 0.07	0.46 ± 0.06	0.28 ± 0.03*
Triglycerides (mg/dL)	104.1 ± 8.1	92.2 ± 10.6	74.9 ± 16.8	63.3 ± 16.1
Cholesterol (mg/dL)	236.9 ± 27.7	230.7 ± 10.8	195.8 ± 31.6	236.8 ± 19.1

Data are mean ± SEM. Serum metabolites, hormones, and lipids were measured after a 6-h fast. T_0 insulin and T_{30} insulin correspond to insulin measured before glucose injection and 30 min after glucose injection, respectively, during GTTs. All other metabolites and hormones were determined by blood samples extracted before glucose injection before GTTs. n = 5 mice per genotype for NCD and n = 8 mice per genotype for HFD. *$P < 0.05$ vs. WT mice under the same feeding condition. **$P < 0.005$ vs. WT mice under the same feeding condition. #$P < 0.05$ vs. NCD within the same genotype. ##$P < 0.005$ vs. NCD within the same genotype.

measured their metabolic rates at various ambient temperatures. At 23°C, VO_2 and VCO_2 were increased in the WT mice on the HFD and in the KO mice independent of the diet, suggesting that the HFD and MnSOD deletion increased the resting metabolic rate (Fig. 4*A* and *D*). Furthermore, when the animals were exposed to a colder temperature (15°C), the VO_2 values increased independent of the diet or genotype but remained higher in the HFD-fed WT mice and in the KO mice independent of the diet (Fig. 4*A* and *D*). By contrast, VCO_2 was increased in all groups at 15°C compared with 23°C but was significantly higher in the KO mice than in the diet-matched WT controls, suggesting that impaired coupling of VO_2 to VCO_2 occurred only in the WT HFD-fed mice (Fig. 4*B* and *E*). Of note, the cold-induced EE was reduced in all groups when the animals were housed at thermoneutrality (30°C), but compared with diet-matched WT controls, the KO mice maintained an increased VO_2 and VCO_2. As for substrate utilization, the HFD-fed WT and KO mice preferably

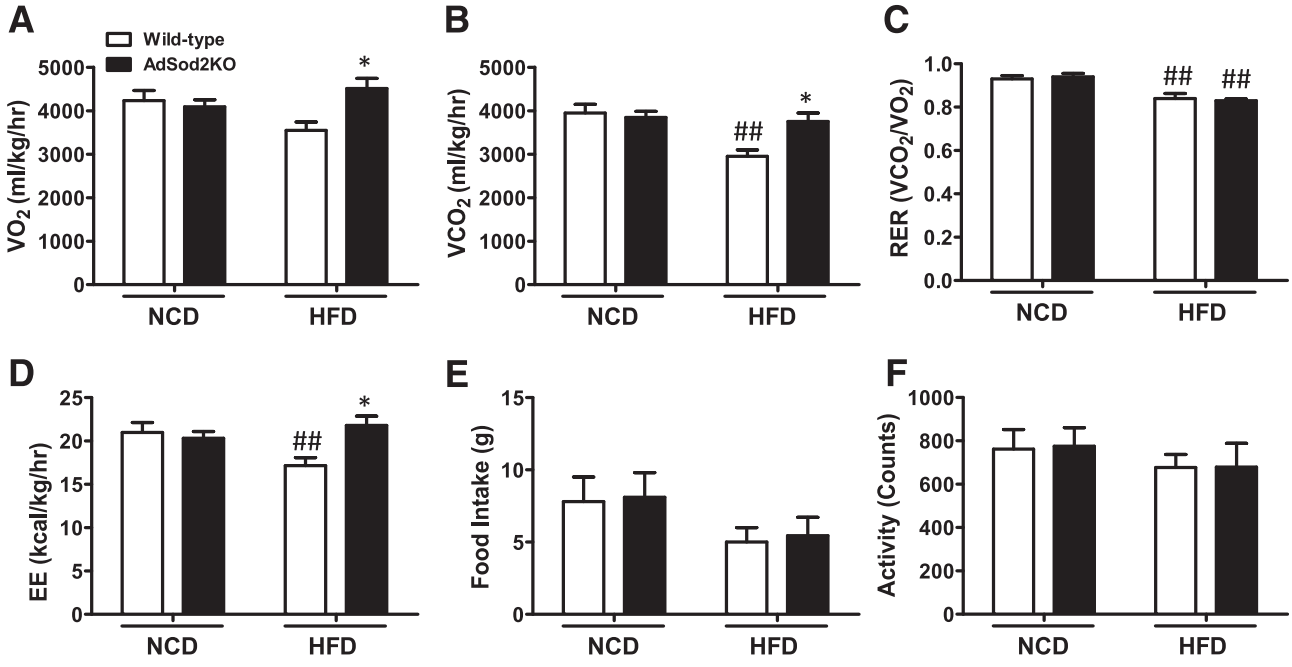

Figure 3—Deletion of MnSOD in adipocytes increased metabolic rate and EE when mice are maintained on an HFD. VO_2 (*A*) and VCO_2 (*B*) at night averaged over a 72-h period. Calculated RER (*C*) and EE (*D*). Food intake (*E*) and ambulatory activity (*F*) in WT and AdSod2 KO mice fed NCD or HFD for 12 weeks. n = 6–9 mice per group. Data are mean ± SEM. *$P < 0.05$ vs. WT under the same feeding condition; ##$P < 0.005$ vs. NCD within the same genotype.

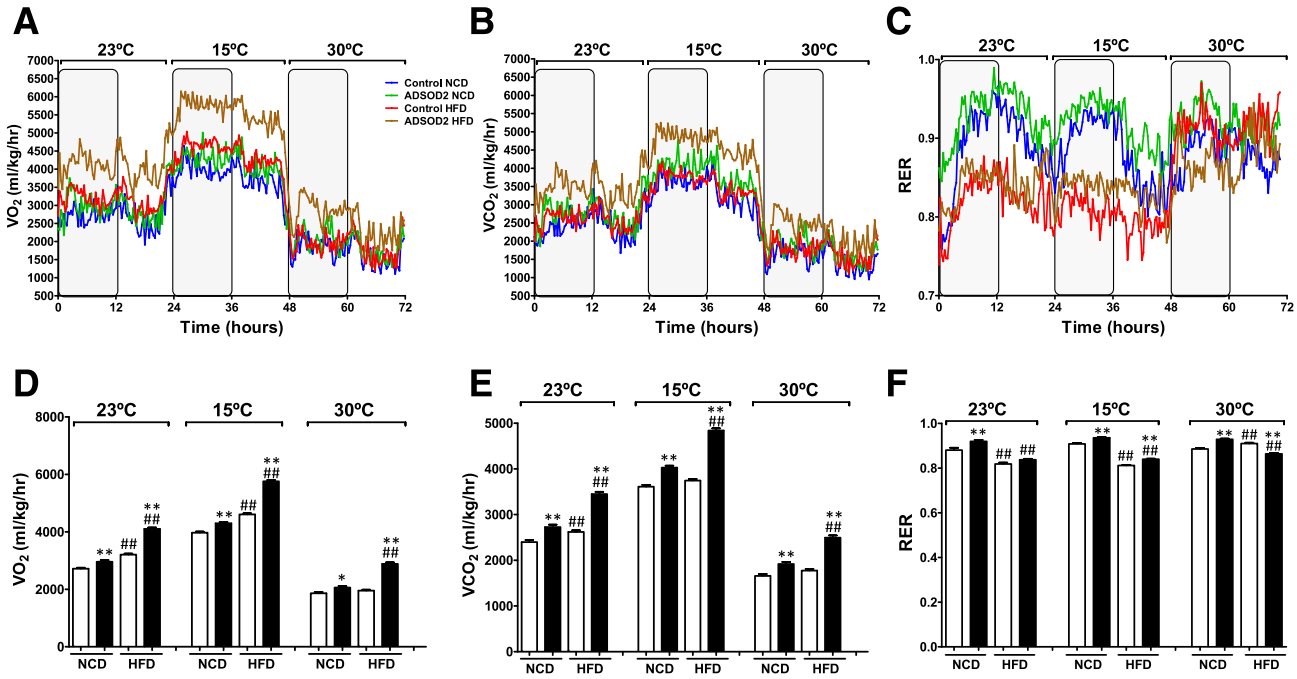

Figure 4—Increased metabolic rate and FA utilization in HFD-fed AdSod2 KO mice at thermoneutrality. WT and AdSod2 KO mice fed NCD or HFD for 8–9 weeks were housed in metabolic cages for 72 h, and their VO_2, VCO_2, and RER were recorded at 23°C, 15°C, and 30°C. *A–C*: Changes in VO_2, VCO_2, and RER, respectively, over 72 h. *D–F*: Average night data for VO_2, VCO_2, and RER, respectively. $n = 4$ mice per group. Data are mean ± SEM. $^*P < 0.05$, $^{**}P < 0.005$ vs. WT under the same feeding condition; $\#\#P < 0.005$ vs. NCD within the same genotype.

used FAs as evidenced by the reduction in the RER at subthermoneutral temperatures (Fig. 4*C* and *F*). By contrast, only the KO mice fed the HFD maintained their reliance on FA utilization when housed at thermoneutrality. Of note, KO mice fed the NCD had the highest RER values at all ambient temperatures, suggesting an impairment in FA utilization despite the higher metabolic rate. Finally, to exclude any contribution from skeletal muscle to the increased metabolic rate observed in the HFD-fed AdSod2 KO mice, we assessed VO_2 and ATP production in saponin-permeabilized soleus fibers and observed no difference between the groups (Supplementary Fig. 6).

FA Oxidation Increases in the iWAT and BAT of HFD-Fed AdSod2 KO Mice

To gain mechanistic insight into the increased metabolic rate and FA utilization observed in the HFD-fed AdSod2 KO mice, we measured palmitate oxidation in BAT, iWAT, and eWAT explants from WT and KO mice fed either the NCD or the HFD for 21 weeks. As depicted in Fig. 5*A*, palmitate oxidation was significantly enhanced in the iWAT and BAT but was unchanged in the eWAT and hindlimb muscle of HFD-fed AdSod2 KO mice compared with HFD-fed WT mice. By contrast, palmitate oxidation was reduced in the eWAT of NCD-fed AdSod2 KO mice compared with NCD-fed WT mice (Supplementary Fig. 5*A*), suggesting a diet-dependent mechanism for increased FA oxidation in the AdSod2 KO mice. In support of enhanced FA oxidation, the mRNA expression of genes involved in FA oxidation (i.e., *Acadvl* and *Ucp3* encoding the very-long-chain acyl-CoA dehydrogenase and UCP-3, respectively) were significantly increased in iWAT and eWAT of the HFD-fed AdSod2 KO mice (Fig. 5*B* and Supplementary Fig. 5*F*). In contrast, none of these changes were observed in iWAT and eWAT of the NCD-fed AdSod2 KO mice compared with diet-matched WT controls (Supplementary Fig. 5*B*).

MnSOD Deletion in Adipocytes Increases Mitochondrial Oxygen Consumption and Biogenesis in the WAT in a Diet-Dependent Manner

Next, we assessed the OCRs in iWAT and eWAT explants from AdSod2 KO and WT mice fed the NCD or HFD by using the Seahorse XF24 Extracellular Flux Analyzer. As shown in Fig. 5*C*, the OCR normalized to the nuclear DNA was increased by twofold in the iWAT of HFD-fed AdSod2 KO mice compared with HFD-fed WT mice. Similarly, OCR in the presence of pyruvate or FCCP was significantly increased in eWAT of AdSod2 KO mice fed HFD compared with WT mice fed the same diet (Supplementary Fig. 5*E*). Given that we observed a higher basal OCR in iWAT, we investigated whether this result was due to increased mitochondrial content. Indeed, we observed a significant 30% increase in mtDNA content normalized to nuclear DNA content in the iWAT of HFD-fed AdSod2 KO mice

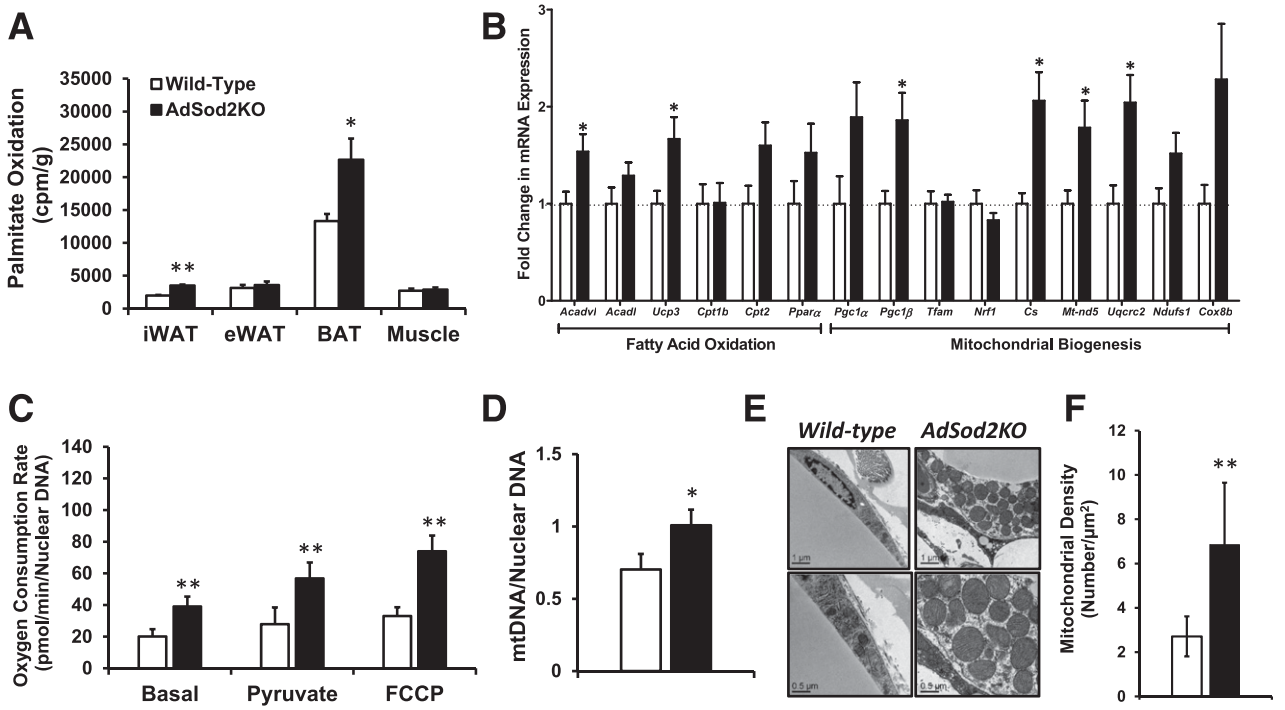

Figure 5—MnSOD deficiency triggered an HFD-dependent increase in FA oxidation, mitochondrial respiration, and mitochondrial biogenesis. WT and AdSod2 KO mice were maintained on an HFD for 21 weeks. *A*: Palmitate oxidation in iWAT, eWAT, BAT, and hindlimb muscle. *B*: Fold change in mRNA expression of FA oxidation and mitochondrial biogenesis genes in iWAT. *C* and *D*: OCR and mtDNA/nuclear DNA ratios in iWAT. *E* and *F*: Electron micrographs and quantification of mitochondrial density in iWAT. n = 8–9 mice per group in *A*, and n = 6 mice per group in *B*. OCR, mtDNA, and mitochondrial density were quantified in three different sections of iWAT from three to four mice per group. Data are mean ± SEM. *$P < 0.05$, **$P < 0.005$ vs. WT. cpm, counts per minute.

compared with that of HFD-fed WT mice (Fig. 5*D*). Furthermore, the mitochondrial volume density was also elevated by more than twofold in the iWAT of HFD-fed AdSod2 KO mice compared with that in HFD-fed WT mice, with no evidence of damaged or swollen mitochondria (Fig. 5*E* and *F*). Consistent with the elevated mtDNA content and volume density, the mRNA levels of key regulators of mitochondrial biogenesis (i.e., peroxisome proliferator–activated receptor γ coactivator [PGC]1α, PGC1β) were elevated by approximately twofold in the iWAT of the KO mice compared with that of the WT mice on the HFD (Fig. 5*B*). Similarly, several transcripts of mitochondrial enzymes and components of the electron transport chain encoded by either the mtDNA or the nuclear DNA were enhanced in the iWAT and eWAT of HFD-fed AdSod2 KO mice, including citrate synthase and subunits of complex I and complex III (Fig. 5*B* and Supplementary Fig. 5*F*). Of note, none of these changes were observed under the NCD condition except for a modest but significant elevation in the *Tfam* mRNA in iWAT of KO mice (Supplementary Fig. 5*B*), suggesting the existence of a diet-dependent transcriptional mechanism for increased mitochondrial biogenesis in the AdSod2 KO mice. In addition to mitochondrial biogenesis, we noted increased mitochondrial fission and reduced mitochondrial fusion in the BAT of KO mice. Evidence for this is increased phosphorylation and activation of the profission protein DRP1 (Supplementary Fig. 1*G* and *H*) and reduced content of the profusion protein MFN-1 (Supplementary Fig. 1*G–I*).

Mitochondrial Uncoupling and mtDNA Content Are Enhanced in Cultured Adipocytes From AdSod2 KO Mice

To test whether the increase in mitochondrial respiration and biogenesis in the iWAT of the AdSod2 KO mice fed the HFD was cell autonomous, we isolated APs from the iWAT of WT and AdSod2 KO mice fed the NCD or HFD for 12 weeks using FACS as previously described (17). Cells that were lineage negative, $CD34^+$, $CD29^+$, and Sca1 positive were differentiated into adipocytes. By day 12 postdifferentiation, MnSOD protein expression was significantly reduced (~80%) in the KO cells (Fig. 6*A*). As expected, lipid accumulation assessed by Oil Red O staining at day 6 postdifferentiation was not affected by the lack of MnSOD (Fig. 6*B* and *C*), indicating that MnSOD deletion using the adiponectin promoter did not alter adipogenesis. Despite the lack of an effect of MnSOD deletion on adipogenesis, superoxide generation was higher in differentiated progenitors from AdSod2 KO mice fed NCD and in HFD-fed WT and KO mice (Fig. 6*D*). Furthermore, the OCR in the presence of the ATP synthase inhibitor

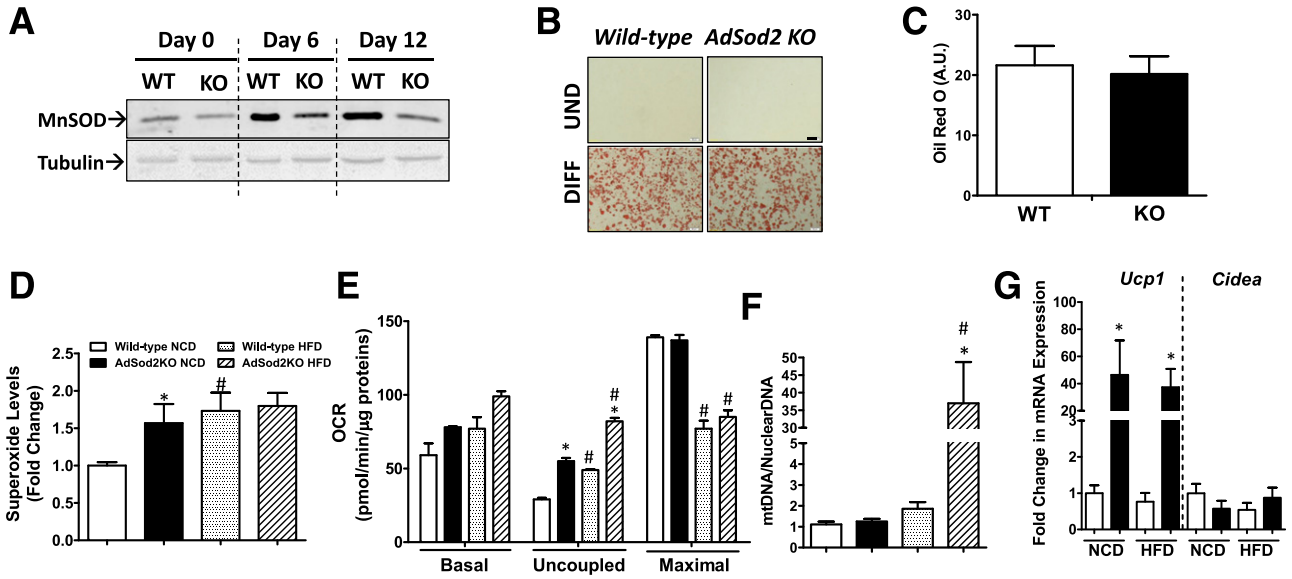

Figure 6—Lack of MnSOD increased superoxide generation, uncoupled respiration, and enhanced mitochondrial content in cultured adipocytes. APs were isolated from iWAT of WT or AdSod2 KO mice fed NCD or HFD for 12 weeks and differentiated into adipocytes. *A*: Representative Western blots of MnSOD and tubulin protein expression before differentiation (day 0) and 6 and 12 days postdifferentiation. Representative images of Oil Red O staining of neutral lipids (*B*) and the corresponding quantification at 6 days postdifferentiation (*C*). Superoxide levels (*D*), OCRs (*E*), and mtDNA/nuclear DNA ratios (*F*) at 12 days postdifferentiation. *G*: Fold change in *Ucp1* and *Cidea* mRNA in iWAT. $n = 3$ independent experiments (each included five to six mice per group). Scale bar = 40 μm in *B*. Data are mean ± SEM. $^*P < 0.05$ vs. WT under the same feeding condition; $\#P < 0.05$ vs. NCD within the same genotype. A.U., arbitrary units; DIFF, differentiated; UND, undifferentiated.

oligomycin, which represents oxygen consumption that is not coupled to ATP synthesis or uncoupled respiration, was increased in the differentiated APs from KO mice fed the NCD and even more so in cells isolated from the HFD-fed KO mice (Fig. 6*E*). Furthermore, when FCCP was added, the OCR was increased to a similar extent in cells from the WT and KO mice on the NCD but was not increased in the KO mice on the HFD, suggesting that their mitochondria were already maximally uncoupled. To examine whether the induction of mitochondrial biogenesis observed in the iWAT explants from KO mice on an HFD also occurred in differentiated APs, we quantified the ratios of mtDNA to nuclear DNA and observed a significant increase in differentiated APs from HFD-fed AdSod2 KO mice (Fig. 6*F*). Because we observed increased uncoupled respiration in APs isolated from the iWAT of KO mice and because of the limited amount of protein we could obtain from these cells, we quantified *Ucp1* and *Cidea* mRNA in the iWAT of WT and KO mice fed the NCD or the HFD and observed a robust induction of *Ucp1* mRNA expression in the iWAT of KO mice that was independent of diet. By contrast, *Cidea* mRNA expression was not significantly altered by diet or genotype (Fig. 6*G*).

Absence of MnSOD in Adipocytes Reduces Hepatic Steatosis, Prevents Adipose Tissue Inflammation, and Preserves Glucose and Insulin Tolerance

Improved metabolism and increased FA oxidation in the WAT and BAT of HFD-fed AdSod2 KO mice led to a significant 40% reduction in circulating FFAs (Table 1). As predicted, HFD-fed WT mice exhibited hepatic steatosis as evidenced by lipid accumulation and an increased triglyceride content; by contrast, this effect was completely prevented in the KO mice fed the same diet (Fig. 7*A* and *B*). Although we did not expect that MnSOD deletion in adipocytes would affect macrophage infiltration in eWAT, we found that the KO mice were completely protected from diet-induced adipose tissue inflammation as assessed by several variables, including quantification of crown-like structures (Supplementary Fig. 7*F* and *G*), F4/80 immunostaining (Fig. 7*C* and *D*), mRNA levels of *Ccl2* and *Il6* (Fig. 7*E*), and MCP1 protein content (Supplementary Fig. 7*H*). Furthermore, the circulating adiponectin levels did not differ between the WT and KO mice on either diet (Table 1). However, because the HFD-fed KO mice had less fat, they may have secreted more adiponectin/fat content. As a result of their improved metabolism, the HFD-fed AdSod2 KO mice exhibited lower fasting glucose and insulin levels and were protected from diet-induced glucose intolerance, even when their body weights were similar to the WT mice after 6 weeks of the HFD (Fig. 7*F–H*); this protection was also observed after 12 weeks on the HFD (Supplementary Fig. 7*D* and *E*). The KO mice also exhibited more insulin sensitivity after 21 weeks on the HFD as demonstrated by an improvement in insulin tolerance (Fig. 7*I* and *J*). Taken together, these data demonstrate that the absence of MnSOD in adipocytes triggers a diet-dependent increase in mitochondrial biogenesis/content

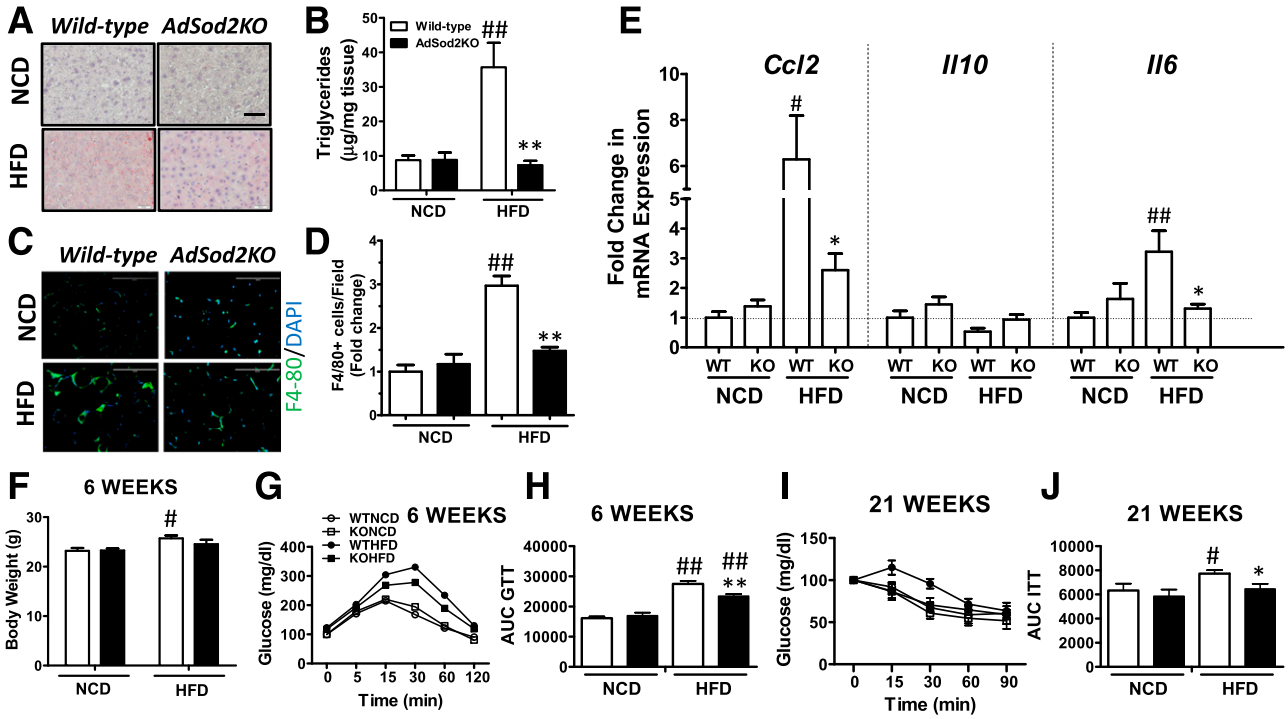

Figure 7—AdSod2 KO mice are protected from diet-induced hepatic steatosis, adipose inflammation, and glucose and insulin intolerance. *A* and *B*: Representative images of liver sections stained with Oil Red O and liver triglyceride content in WT and AdSod2 KO mice fed NCD and HFD for 21 weeks. *C* and *D*: Macrophage (F4/80) staining and quantification in eWAT. *E*: Fold change in mRNA expression of pro- and anti-inflammatory genes in eWAT. *F–H*: Body weights, GTTs, and areas under the curve (AUCs) for GTT in WT and AdSod2 KO mice fed NCD or HFD for 6 weeks. *I* and *J*: Insulin tolerance tests (ITTs) and AUCs for ITT in WT and AdSod2 KO mice fed NCD or HFD for 21 weeks. n = 4–5 mice per group for *A–D*, n = 6 mice per group for *E*, and n = 8–17 mice per group for *F–J*. Scale bars = 20 μm in *A* and 400 μm in *C*. Data are mean ± SEM. $^*P < 0.05$, $^{**}P < 0.005$ vs. WT under the same feeding condition; #$P < 0.05$, ##$P < 0.005$ vs. NCD within the same genotype.

and FA oxidation, leading to the clearance of circulating FFAs and the preservation of insulin sensitivity during HFD feeding.

DISCUSSION

In healthy mitochondria, MnSOD dismutates superoxide anions generated as a by-product of the electron transport chain to the strong oxidant H_2O_2 (18), which is subsequently transformed into water by catalase, glutathione peroxidase, peroxiredoxin, or thioredoxins. Thus, MnSOD functions as a critical regulator of mitochondrial-driven ROS signaling in the cell. We developed a novel mouse model with increased mitochondrial superoxide generation by deleting MnSOD in fat cells. This model addresses the role of mitochondrial superoxide in the function of mature adipocytes without its confounding effect on adipogenesis. The results demonstrate that deletion of MnSOD by using the adiponectin promoter did not affect lipid accumulation in the differentiated APs (Fig. 6). The absence of MnSOD enhanced superoxide levels in white adipocytes from KO mice and HFD-fed WT mice, but protein carbonylation did not differ between the groups in either fat depot. This finding conflicts with published results showing HFD-induced protein carbonylation in eWAT but not in iWAT (19). The assay we used, which was based on the use of an antibody directed toward 4-HNE protein Michael adducts, possibly was less sensitive than the liquid chromatography–tandem mass spectrometry approach that was previously used. However, consistent with published data (19), we observed a robust reduction in mRNA expression of *Gsta4*, which is a key enzyme involved in 4-HNE detoxification in both iWAT and eWAT of WT mice fed an HFD. Although the *Gsta4* mRNA recovered in the HFD-fed KO mice, the difference was not significant. The lack of oxidative damage and the induction of antioxidant defense mechanisms in adipose tissue of HFD-fed AdSod2 KO mice could have resulted from reduced H_2O_2 levels from the absence of MnSOD. Although we did not measure H_2O_2 in the samples, a compensatory increase in the protein expression of enzymes involved in its detoxification, such as catalase or GPX4, was not evident.

Despite the clear association between OS and obesity, the role of the adipocyte mitochondrial superoxide in fat expansion, whole-body energy homeostasis, and insulin sensitivity in vivo has never been examined. By generating adipocyte-specific MnSOD-deficient mice, we aimed to determine whether mitochondrial superoxide generation exacerbated diet-induced obesity and insulin resistance. Instead, the AdSod2 KO mice were protected against

diet-induced adiposity and insulin resistance. The lean phenotype of the AdSod2 KO mice was diet dependent because the animals on the NCD maintained the same body weight and adiposity as their corresponding WT controls when housed at 23°C. Furthermore, differences in fat accrual did not manifest until ~8–9 weeks on the HFD in the AdSod2 KO mice, suggesting the development of an adaptive response over time. A diet-dependent reduction in the iWAT and eWAT was observed in the HFD-fed AdSod2 KO mice, but the BAT was atrophied in the KO mice independent of diet. The mechanisms underlying the reduced BAT size are not fully understood, but this finding resembles the observation of BAT involution in mice overexpressing UCP-1 under the control of the aP2 promoter (20). Similar to aP2-UCP-1 transgenic mice, we found that BAT atrophy was caused by reduced cellularity and was not associated with the decreased UCP-1 content. Indeed, UCP-1 immunostaining revealed an increase in BAT of the HFD-fed AdSod2 KO mice (Supplementary Fig. 3*E* and *F*). Because BAT atrophy was observed independent of diet, that it was caused by the compensatory increase in the metabolic rate, which was higher in the white fat of the HFD-fed KO mice, is unlikely. Therefore, atrophy could be the result of impaired proliferation and/or enhanced cell death of brown adipocytes. These possibilities are currently under investigation.

Reduced adiposity in the HFD-fed KO mice was not caused by excessive caloric intake or activity-driven EE; instead, it was the consequence of an increased metabolic rate as evidenced by the higher VO_2 and VCO_2 values even when the animals were housed at thermoneutrality. These data demonstrate that the mechanism underlying the increased EE in the AdSod2 KO mice is not due to a compensatory increase in adaptive thermogenesis to preserve body temperature. Despite the increased metabolic rate in the KO mice fed the NCD for 8 weeks, these animals, compared with KO mice maintained on an HFD, failed to lose weight. One explanation for this finding is the inability of the NCD-fed KO mice to use FAs as evidenced by the higher RER values at all temperatures tested (Fig. 4). When we examined FA oxidation in adipose explants, only the HFD-fed KO mice had higher palmitate oxidation in both the iWAT and the BAT, whereas the NCD-fed KO mice exhibited a decrease in palmitate oxidation in the eWAT. As a result of increased FA oxidation in the WAT and BAT of the HFD-fed KO mice, circulating FFAs were reduced by >40%. By contrast, circulating FFAs trended higher in the NCD-fed KO mice, enforcing the hypothesis that KO mice on the NCD were not using FAs. Despite the increase in FA oxidation in iWAT, adipocyte diameter was not changed, which could be due to elevated FA uptake and/or FA synthesis to compensate for the increase in FA oxidation. Alternatively, the findings could be secondary to a reduction in lipolysis, thus creating futile FA cycling, a mechanism shown previously to be operational in adipocytes (21).

The mechanisms underlying increased FA oxidation in the HFD-fed KO mice are not completely known but could involve increased expression of genes involved in FA metabolism. Another possibility is the overall increase in the mitochondrial oxidative capacity and number that were only observed in the HFD-fed KO mice. These findings were reproduced in isolated and differentiated APs from the HFD-fed KO mice, suggesting a cell autonomous response to the lack of MnSOD. Indeed, differentiated progenitors from iWAT of AdSod2 KO mice fed NCD exhibited higher superoxide levels than those of diet-matched WT mice. However, this increase, which persisted with HFD, was no longer different between the groups, which could be due to the higher induction of mitochondrial uncoupling of oxidative phosphorylation observed in differentiated progenitors from the iWAT of HF-fed KO mice. Currently, whether the increase in mitochondrial oxygen consumption is due to coupled or uncoupled respiration is unclear. However, when differentiated progenitors were used, the OCR measured in the absence of ATP synthesis (uncoupled respiration) was highest in cells from HFD-fed KO mice. Furthermore, the same cells were unable to further increase their OCRs after the addition of the artificial uncoupler FCCP, suggesting that they had already reached their maximal uncoupling capacity. This uncoupling capacity observed more in the cells issued from HF-KO mice occurred despite similar induction of *Ucp1* mRNA in iWAT isolated from KO mice on both NCD and HFD. These results suggest the existence of an activation mechanism that occurs only in progenitors from HF-fed KO mice. Indeed, previous studies have implicated both superoxide and FA as potential activators of the UCP-1 protein (22). Thus, the combination of increased superoxide generation and FA in the setting of *Ucp1* mRNA induction could have resulted in the activation of uncoupling. The mechanisms underlying *Ucp1* mRNA induction in iWAT of KO mice are not fully understood; this increase especially is specific to *Ucp1* because other genes involved in browning (i.e., *Cidea*) were not changed, suggesting a novel mechanism for *Ucp1* induction in adipocytes lacking MnSOD. Consistent with the current results, a recent study revealed that UCP-1 content was elevated in skin tissues from Sod2 heterozygous mice and that this induction was mediated through ROS-peroxisome proliferator–activated receptor-α signaling (23). Consistent with this hypothesis, UCP-1 expression was induced in the BAT and WAT of mouse models with increased ROS generation (7,24,25). Taken together, these results suggest the existence of ROS-mediated signaling that regulates UCP-1 expression, which warrants further investigation.

An additional finding from this work was that the lack of MnSOD in adipocytes triggered diet-dependent mitochondrial biogenesis. The mechanisms involved in this increase could be *1*) the induction of a mitochondrial biogenesis transcriptional regulator, such as PGC1α and PGC1β; *2*) alterations in the redox state of the cells; and/or *3*) changes in calcium homeostasis. Indeed, earlier work showed that PGC1α and PGC1β can be induced by

OS in cells and that cells lacking PGC1α cannot recover their mitochondrial function after loss of ATP through mitochondrial uncoupling (26,27). Furthermore, human cells respond to defective respiratory functions by promoting the expression of nuclear and mitochondrial genes through an H_2O_2-dependent signaling pathway (28). Conversely, the depletion of mtDNA below a certain threshold increased steady-state levels of cytosolic calcium, which might alter calcium-dependent transcription factors, such as nuclear factor of activated T cells, activating transcription factor 2, and nuclear factor-κB. Thus, both mtDNA mutation/depletion and metabolic stress in mammalian cells are proposed to transmit a retrograde Ca^{2+} signal, which subsequently alters the expression of nuclear oxidative phosphorylation genes and mitochondrial biogenesis genes (29). Indeed, we observed a coordinated induction of mtDNA and nuclear DNA–encoded genes only in the HFD-fed KO mice (Fig. 5*B*). However, why mitochondrial biogenesis was only observed in the HFD-fed KO mice and not in the NCD-fed KO mice or in the HFD-fed WT mice despite the higher levels of superoxide production is unclear. One possible explanation could be the amount of superoxide generated. A positive correlation between the amount of ROS and the mtDNA content in cells was previously reported (30). Furthermore, other reactive species could be specifically produced in HFD-fed KO mice that might trigger this response, such as peroxynitrate, which was shown to induce mitochondrial biogenesis in kidney cells lacking MnSOD (31). In addition to the induction of mitochondrial biogenesis observed in iWAT of HF-fed AdSod2 KO mice, the current results suggest that MnSOD deletion in BAT adipocytes triggered mitochondrial fragmentation characterized by DRP1 phosphorylation. Consistent with increased mitochondrial fission with MnSOD deletion, mitochondrial fusion was significantly inhibited, especially under the HFD condition. The underlying mechanisms for altered mitochondrial dynamics in BAT adipocytes with MnSOD deletion is not fully understood but could result from the sustained activation of mitochondrial uncoupling. Indeed, a similar mitochondrial fragmentation was observed in brown adipocytes stimulated by norepinephrine (32).

Finally, as expected from increased EE and higher FA oxidation rates, AdSod2 KO mice were protected from diet-induced hepatic steatosis and glucose and insulin intolerance. The maintenance of insulin sensitivity in AdSod2 KO mice on HFD could be the result of decreased circulating FFA and preserved adiponectin. Furthermore, we assumed that increased mitochondrial OS would lead to more chronic inflammation in eWAT, but we found that AdSod2 KO mice were protected from diet-induced inflammation. Although this could still be the consequence of increased FA oxidation and FFA clearance, which may limit the formation of lipid peroxides known to promote adipose inflammation (33), other mechanisms could be involved. In summary, the current results demonstrate that manipulation of OS in fat cells, through deletion of MnSOD, triggers several stress response mechanisms, including mitochondrial biogenesis and mitochondrial oxidation of FA and/or uncoupling, to protect mice from diet-induced fat accumulation and insulin resistance.

Acknowledgments. The authors thank the Metabolic Phenotyping Core Facility (University of Utah) for its assistance with the CLAMS and the Seahorse studies. They also thank John David Symons (University of Utah) for help with reading and editing the revised manuscript.

Funding. This work was supported by National Institute of Diabetes and Digestive and Kidney Diseases grants 1-R01-DK-098646-01A1 and R01-DK-099110. K.M.P. is supported by an American Heart Association postdoctoral fellowship (15POST25360014). This work was also supported by Scientist Development Grant 09SDG2220218 from the American Heart Association to S.B.

Duality of Interest. No potential conflicts of interest relevant to this article were reported.

Author Contributions. Y.H.H., M.B., K.M.P., and S.P. contributed to the data collection and analysis. P.E.S. contributed the adiponectin-*Cre* mice. S.B. contributed to the study conception and design and writing of the manuscript. S.B. is the guarantor of this work and, as such, had full access to all the data in the study and takes responsibility for the integrity of the data and the accuracy of the data analysis.

References

1. Keaney JF Jr, Larson MG, Vasan RS, et al.; Framingham Study. Obesity and systemic oxidative stress: clinical correlates of oxidative stress in the Framingham Study. Arterioscler Thromb Vasc Biol 2003;23:434–439

2. Furukawa S, Fujita T, Shimabukuro M, et al. Increased oxidative stress in obesity and its impact on metabolic syndrome. J Clin Invest 2004;114:1752–1761

3. Lee YS, Kim AY, Choi JW, et al. Dysregulation of adipose glutathione peroxidase 3 in obesity contributes to local and systemic oxidative stress. Mol Endocrinol 2008;22:2176–2189

4. Frohnert BI, Sinaiko AR, Serrot FJ, et al. Increased adipose protein carbonylation in human obesity. Obesity (Silver Spring) 2011;19:1735–1741

5. Huh JY, Kim Y, Jeong J, et al. Peroxiredoxin 3 is a key molecule regulating adipocyte oxidative stress, mitochondrial biogenesis, and adipokine expression. Antioxid Redox Signal 2012;16:229–243

6. Giorgio M, Migliaccio E, Orsini F, et al. Electron transfer between cytochrome c and p66Shc generates reactive oxygen species that trigger mitochondrial apoptosis. Cell 2005;122:221–233

7. Berniakovich I, Trinei M, Stendardo M, et al. p66Shc-generated oxidative signal promotes fat accumulation. J Biol Chem 2008;283:34283–34293

8. Liu Y, Qi W, Richardson A, Van Remmen H, Ikeno Y, Salmon AB. Oxidative damage associated with obesity is prevented by overexpression of CuZn- or Mn-superoxide dismutase. Biochem Biophys Res Commun 2013;438:78–83

9. Lark DS, Kang L, Lustig ME, et al. Enhanced mitochondrial superoxide scavenging does not improve muscle insulin action in the high fat-fed mouse. PLoS One 2015;10:e0126732

10. Tormos KV, Anso E, Hamanaka RB, et al. Mitochondrial complex III ROS regulate adipocyte differentiation. Cell Metab 2011;14:537–544

11. Hwang J, Saha A, Boo YC, et al. Oscillatory shear stress stimulates endothelial production of O2- from p47phox-dependent NAD(P)H oxidases, leading to monocyte adhesion. J Biol Chem 2003;278:47291–47298

12. Pires KM, Ilkun O, Valente M, Boudina S. Treatment with a SOD mimetic reduces visceral adiposity, adipocyte death, and adipose tissue inflammation in high fat-fed mice. Obesity (Silver Spring) 2014;22:178–187

13. Wang RH, Li C, Deng CX. Liver steatosis and increased ChREBP expression in mice carrying a liver specific SIRT1 null mutation under a normal feeding condition. Int J Biol Sci 2010;6:682–690

14. Boudina S, Sena S, Sloan C, et al. Early mitochondrial adaptations in skeletal muscle to diet-induced obesity are strain dependent and determine oxidative stress and energy expenditure but not insulin sensitivity. Endocrinology 2012;153:2677–2688
15. Luo B, Parker GJ, Cooksey RC, et al. Chronic hexosamine flux stimulates fatty acid oxidation by activating AMP-activated protein kinase in adipocytes. J Biol Chem 2007;282:7172–7180
16. Oruganty-Das A, Ng T, Udagawa T, Goh EL, Richter JD. Translational control of mitochondrial energy production mediates neuron morphogenesis. Cell Metab 2012;16:789–800
17. Rodeheffer MS, Birsoy K, Friedman JM. Identification of white adipocyte progenitor cells in vivo. Cell 2008;135:240–249
18. McCord JM, Fridovich I. Superoxide dismutase. An enzymic function for erythrocuprein (hemocuprein). J Biol Chem 1969;244:6049–6055
19. Long EK, Olson DM, Bernlohr DA. High-fat diet induces changes in adipose tissue trans-4-oxo-2-nonenal and trans-4-hydroxy-2-nonenal levels in a depot-specific manner. Free Radic Biol Med 2013;63:390–398
20. Stefl B, Janovská A, Hodný Z, et al. Brown fat is essential for cold-induced thermogenesis but not for obesity resistance in aP2-Ucp mice. Am J Physiol 1998;274:E527–E533
21. Flachs P, Rossmeisl M, Kuda O, Kopecky J. Stimulation of mitochondrial oxidative capacity in white fat independent of UCP1: a key to lean phenotype. Biochim Biophys Acta 2013;1831:986–1003
22. Echtay KS, Roussel D, St-Pierre J, et al. Superoxide activates mitochondrial uncoupling proteins. Nature 2002;415:96–99
23. Xu Y, Miriyala S, Fang F, et al. Manganese superoxide dismutase deficiency triggers mitochondrial uncoupling and the Warburg effect. Oncogene 2015;34:4229–4237
24. Schneider K, Valdez J, Nguyen J, et al. Increased energy expenditure, UCP1 expression and resistance to diet-induced obesity in mice lacking nuclear factor-erythroid-2 related transcription factor-2 (Nrf2). J Biol Chem 2016;291:7754–7766
25. Ro SH, Nam M, Jang I, et al. Sestrin2 inhibits uncoupling protein 1 expression through suppressing reactive oxygen species. Proc Natl Acad Sci U S A 2014;111:7849–7854
26. St-Pierre J, Drori S, Uldry M, et al. Suppression of reactive oxygen species and neurodegeneration by the PGC-1 transcriptional coactivators. Cell 2006;127:397–408
27. Rohas LM, St-Pierre J, Uldry M, Jäger S, Handschin C, Spiegelman BM. A fundamental system of cellular energy homeostasis regulated by PGC-1alpha. Proc Natl Acad Sci U S A 2007;104:7933–7938
28. Suzuki H, Kumagai T, Goto A, Sugiura T. Increase in intracellular hydrogen peroxide and upregulation of a nuclear respiratory gene evoked by impairment of mitochondrial electron transfer in human cells. Biochem Biophys Res Commun 1998;249:542–545
29. Biswas G, Adebanjo OA, Freedman BD, et al. Retrograde Ca2+ signaling in C2C12 skeletal myocytes in response to mitochondrial genetic and metabolic stress: a novel mode of inter-organelle crosstalk. EMBO J 1999;18:522–533
30. Moreno-Loshuertos R, Acín-Pérez R, Fernández-Silva P, et al. Differences in reactive oxygen species production explain the phenotypes associated with common mouse mitochondrial DNA variants. Nat Genet 2006;38:1261–1268
31. Marine A, Krager KJ, Aykin-Burns N, Macmillan-Crow LA. Peroxynitrite induced mitochondrial biogenesis following MnSOD knockdown in normal rat kidney (NRK) cells. Redox Biol 2014;2:348–357
32. Wikstrom JD, Mahdaviani K, Liesa M, et al. Hormone-induced mitochondrial fission is utilized by brown adipocytes as an amplification pathway for energy expenditure. EMBO J 2014;33:418–436
33. Frohnert BI, Bernlohr DA. Glutathionylated products of lipid peroxidation: a novel mechanism of adipocyte to macrophage signaling. Adipocyte 2014;3:224–229